Catalytic hollow fiber membranes prepared using layer-by-layer adsorption of polyelectrolytes and metal nanoparticles

Lu Ouyang [a], David M. Dotzauer [a], Seth R. Hogg [a], Jorge Macanás [b],
Jean-Francois Lahitte [b], Merlin L. Bruening [a],*

[a] Department of Chemistry, Michigan State University, East Lansing, MI 48824, United States
[b] Laboratoire de Génie Chimique, Université Paul Sabatier, 118 route de Narbonne, 31062 Toulouse Cedex, France

ARTICLE INFO

ABSTRACT

Immobilization of metal nanoparticles in hollow fiber membranes via alternating adsorption of polyelectrolytes and negatively charged Au nanoparticles yields catalytic reactors with high surface areas. SEM images show that this technique deposits a high density of unaggregated metal nanoparticles both on the surfaces and in the pores of the hollow fibers. Catalytic reduction of 4-nitrophenol with NaBH$_4$, which can be easily monitored by UV–vis spectrophotometry, demonstrates that the nanoparticles in the hollow fiber membrane are highly catalytically active. In a single pass through the membrane, >99% of the 4-nitrophenol is reduced to 4-aminophenol, but this conversion decreases over time. The conversion decline may stem from catalyst fouling caused by by-products of 4-aminophenol oxidation.

© 2010 Elsevier B.V. All rights reserved.

1. Introduction

Hollow fiber membrane reactors, which initially appeared in the 1980s [1–4], are attractive because their geometry provides a high surface area to volume ratio [5–7] and should facilitate gas–liquid reactions [8–10]. Moreover, the hollow fiber module is the membrane configuration with the highest packing density. Remarkably, the ratio of membrane surface area to module volume can reach values as high as 30,000 m^2/m^3 [11]. Thus, a number of recent studies examine hollow fibers as catalyst supports in membrane reactors [8,12–15].

Metal nanoparticles are especially effective catalysts because of their relatively large percentage of surface atoms [16,17]. Additionally, these materials often possess unusual electronic properties due to their unique size, which is between the bulk and molecular regimes [16–18]. For most practical catalytic applications, however, the nanoparticles must be immobilized on solid supports to prevent aggregation and facilitate catalyst recovery [16,19–25]. Common methods for making supported noble metal catalysts include impregnation, coprecipitation (CP) and deposition-precipitation (DP) [26]. In impregnation, the support is typically immersed into a metal salt solution and heated in air, and the adsorbed metal species are reduced in hydrogen [27–29]. For the CP [30,31] or DP methods [30,32], the noble metal precursor is either coprecipitated with support precursor or directly deposited on the support sur-face prior to precipitation with another reagent. These methods usually yield metal particles of non-uniform size and shape, and the degree of catalyst dispersion depends on various factors such as the type of support, the deposition pH and the concentration of precursors in the solutions [26,27,33]. To make heterogeneous catalysts with more control over particle size and shape, metal nanoparticles can be synthesized in solution and then loaded on the support [20,34].

Layer-by-layer (LBL) deposition of polycations and polyanions provides a particularly simple way to deposit a high density of well-defined metal nanoparticles on a wide range of substrates [35–40]. Alternating adsorption of charged nanoparticles and an oppositely charged polyelectrolyte affords control over the amount of nanoparticles deposited through variation of the number of adsorbed layers, and a wide range of particle sizes and compositions are available through tuning of the nanoparticle synthesis [41–45]. The LBL technique is effective for membrane modification because it can occur on a wide variety of substrate geometries [46], including flat surfaces, cylindrical particles, and the pores of flat sheet membranes [35,41,42,45].

This paper describes modification of hollow fiber microfiltration (MF) membranes through LBL adsorption of polyelectrolytes and citrate-stabilized metal nanoparticles (NPs) to create reactors that catalyze the reduction of 4-nitrophenol with NaBH$_4$ (Fig. 1). An article by Macanás et al. (in this issue) focuses mostly on coating the surfaces of fibers with nanoparticles [47], whereas this study aims to modify the interior and exterior of the membrane to increase nanoparticle loading.

* Corresponding author. Tel.: +1 517 355 9715x237; fax: +1 517 353 1793.
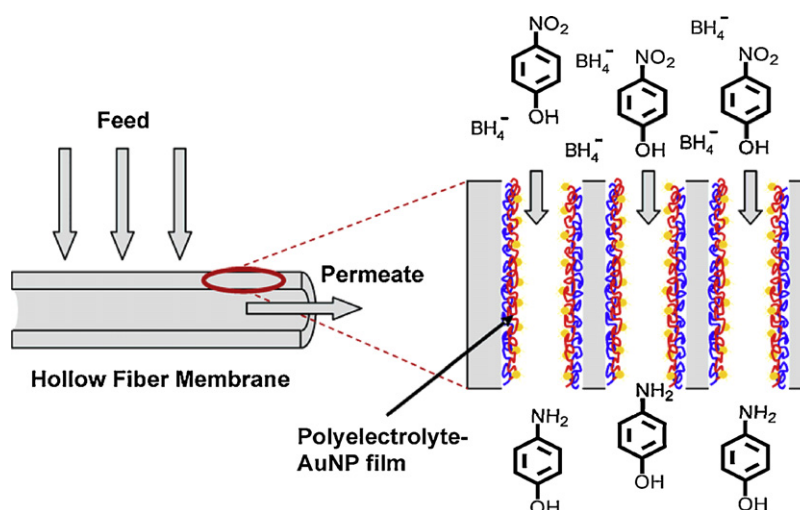*E-mail address:* bruening@chemistry.msu.edu (M.L. Bruening).

Fig. 1. Schematic diagram of a porous hollow fiber membrane modified with a polyelectrolyte/AuNP film. The fibers serve as catalytic reactors for the reduction of 4-nitrophenol by $NaBH_4$.

2. Experimental

2.1. Materials

Poly(sodium 4-styrenesulfonate) (PSS, M_w = 70,000 Da), poly (allylamine hydrochloride) (PAH, M_w = 56,000 Da), $HAuCl_4 \cdot 3H_2O$, sodium citrate, $NaBH_4$ and 4-nitrophenol were used as received from Sigma–Aldrich. Deionized water (Milli-Q purification system, 18.2 MΩ cm) was employed for membrane rinsing and preparation of polyelectrolyte or reaction solutions, and the pH of the PAH solutions was adjusted with dilute HCl or NaOH.

Polyethersulfone (PES) MF hollow fiber membranes (MicroPES Capillary membrane Type TF10) were manufactured by MEM-BRANA (Wuppertal, Germany). These membranes have a specified maximum pore size in the membrane skin of 0.5 ± 0.1 μm, an inner diameter of 300 ± 40 μm and a wall thickness of 100 ± 25 μm.

A module containing MF polysulfone (PS) hollow fiber membranes was purchased from GE Healthcare (Model #: CFP-6-D-6A), and individual fibers were removed from the module and repotted. The fibers have an average skin pore size of 0.65 μm, an inner diameter of 750 μm and a wall thickness of 225 μm. The supplementary material contains SEM images of these fibers (Supplementary data, Fig. S1).

2.2. Preparation of citrate-stabilized Au nanoparticles

Au nanoparticles were prepared by the citrate reduction method [18,48,49], where citrate serves as both the reducing agent and the nanoparticle stabilizer. In a 250 mL round-bottom flask equipped with a condenser, 100 mL of 1 mM $HAuCl_4$ solution was heated to a rolling boil while stirring. Ten mL of 38.8 mM sodium citrate solution was also heated to a rolling boil and then rapidly added to the Au solution. After about 15 s, the solution changed from colorless to blue and then burgundy. The mixture was subsequently stirred with heating for another 10 min, and then without heating for 15 min. The nanoparticle solution was kept in an amber glass bottle and stored in a refrigerator until use. Prior to particle deposition, the nanoparticle solution was diluted 9:1 with deionized water. TEM images show that the particle diameter is 12 ± 1 nm [42].

2.3. Modification of hollow fiber membranes

Following a literature procedure, the hollow fibers were potted in a PVC tube with epoxy glue purchased from Axson Technologies (Cat. Number: Adekit A 130) [50]. All the modules in this study contained one fiber, with an effective fiber length (distance between the potting glue on the two ends) of about 22 cm for PES fibers and 15 cm for PS fibers. Prior to modification, the potted PES fiber was rinsed with water at 0.7 bar for 30 min. In the modification steps, all the solutions were passed through the membrane in the lumen to shell flow configuration with cross-flow (see Fig. 2) using a pressure of 0.7 bar. Cross-flow was used during modification in an effort to minimize any pore blockage caused by the polyelectrolytes. A prefilter (2.5 μm Ahlstrom qualitative filter paper) was used to remove small particles that can potentially block the fiber, and this filter paper was replaced after deposition of each layer. Polyelectrolyte adsorption solutions contained 2 mM PSS or PAH and 50 mM NaCl (polyelectrolyte concentrations are always given with respect to the repeating unit). The pH of the PAH solution was adjusted to 4.5. The modification started with passage of 100 mL of PSS solution through the fiber (volume includes both transmembrane and cross-flow). This initial adsorption of PSS is likely driven by hydrophobic interactions between PSS and the PES fiber [51,52]. The fiber was then rinsed with 300 mL of water to remove any extra polyelectrolytes. Subsequently, 100 mL of PAH solution was passed through the hollow fiber membrane followed by another 300 mL water rinse. Nanoparticles were loaded by passing 100 mL of citrate-stabilized Au colloid solution (~0.1 mM in Au atoms) through the membrane prior to rinsing with 300 mL of water. The permeate of the nanoparticle solution was initially colorless and then became light pink when the fiber was nearly saturated with Au nanoparticles. Modification of the PS fiber occurred in a similar
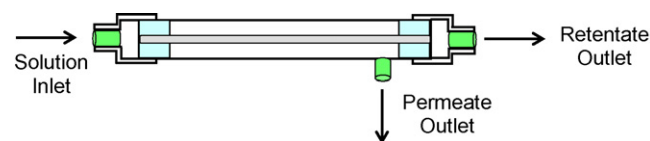

Fig. 2. Schematic diagram of the flow configuration for modifying a hollow fiber membrane with a PSS/PAH/AuNP film. Flow occurs both axially along the membrane and from the inside to the outside of the fiber.
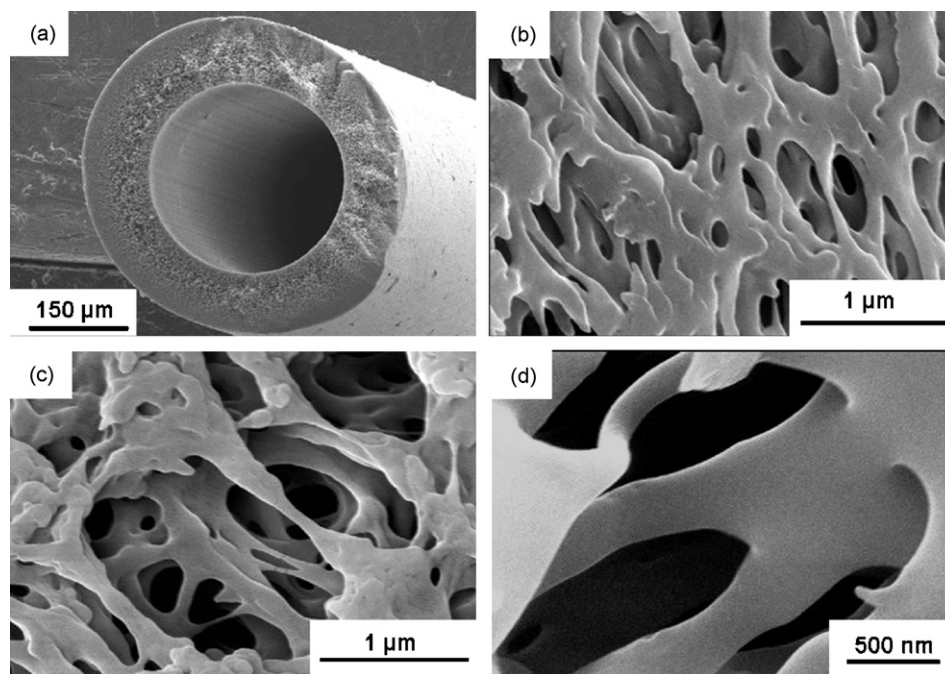
Fig. 3. SEM images of a bare PES hollow fiber membrane. (a) Cross-section of the entire hollow fiber, (b) shell surface, (c) lumen surface and (d) the interior of the membrane.

fashion with slight modifications, and the supplementary material contains the detailed procedure.

2.4. Membrane characterization

SEM images of bare and coated hollow fiber membranes were taken using a Hitachi S-4700 II field-emission scanning electron microscope (FESEM). For shell and lumen surface characterization, 5 nm of Au was sputter-coated (Pelco SC-7 auto sputter coater) on the surface before imaging. For cross-sectional images, the fiber was dipped in ethanol for 2 min, fractured in liquid nitrogen, and the cross-section was sputter-coated with 5 nm of Au.

To determine the amount of Au loaded in the fiber, the membrane was immersed in aqua regia (3 parts HCl and 1 part HNO_3) for 5 min, and this solution was then diluted and analyzed for Au by atomic absorption spectroscopy (AAS) (Varian Spectra Atomic Absorption-200 Spectrometer).

The water permeability of the PES fiber was tested in a shell to lumen flow configuration (no cross-flow in the shell) at room temperature with pressures ranging from 0.7 to 2.1 bars. All fluxes reported in this work are calculated with respect to the surface area of the outside of the fiber. Hydraulic permeability values, which were obtained from the slopes of plots of flux versus pressure, were determined before and after each modification step. For the PS fiber, water permeability was determined only at 0.7 bar because the membrane manufacturer does not recommend using the fibers under pressures higher than 1 bar.

2.5. Catalytic reactions and leaching studies

Reduction of aqueous 4-nitrophenol with $NaBH_4$ served as a model reaction for examining the catalytic activity of the modified membranes. A feed tank was filled with 0.5–1 L of a freshly prepared solution containing 0.5 mM 4-nitrophenol and 25 mM $NaBH_4$, and this solution was forced through the hollow fiber membrane under pressure. Permeate samples were collected every 5 or 10 min, and the concentration of 4-nitrophenol in the feed and permeate was determined from the solution absorbance at 400 nm [42,53] (UV–vis spectra were acquired with a Perkin-Elmer Lambda

40 spectrophotomer.) To examine the extent of catalyst leaching during the reaction, the amount of Au in the feed and permeate samples was determined using inductively coupled plasma optical emission spectroscopy (ICP-OES) (Varian 710-ES ICP Optical Emission Spectrometer). Residence time is calculated with an assumption of 30% porosity.

3. Results and discussion

3.1. Membrane characterization

The first sign of successful modification of the hollow fiber membranes with Au nanoparticles is a change in the fiber color from white to red. SEM images, elemental analysis by AAS, and water permeability measurements afford a more quantitative picture of the fiber modification.

3.2. SEM characterization of immobilized nanoparticles

Fig. 3 shows SEM images of bare PES hollow fiber membranes. These fibers have a layered, porous structure on both lumen and shell sides, but pore sizes are smallest at the shell surface and largest in the interior of the fiber. The extensive internal surface area of the membrane pores should allow a high loading of Au nanoparticles, and the relatively large pores (maximum pore size around 2 μm) facilitates film adsorption without pore blockage. However, pore blockage sometimes occurs, especially in fiber sections that contain somewhat smaller pores (see below). Fig. 4 shows SEM images of the shell, lumen and wall surfaces of PES hollow fiber membranes modified with PSS/PAH/AuNP films. Adsorption of the films occurs by flowing solution along the lumen side of the fiber and also through the fiber wall as described in Section 2.3. Consequently, nanoparticles appear on all surfaces of the membranes. The nanoparticles are well separated with no apparent aggregation, and the particle size is about 12 nm, which is consistent with TEM images of the as-prepared particles [41,42]. Fig. 5 and Supplementary data, Fig. S2 show that modification of PS fibers with PSS/PAH/AuNP films results in a similar, uniform Au nanoparticle distribution.
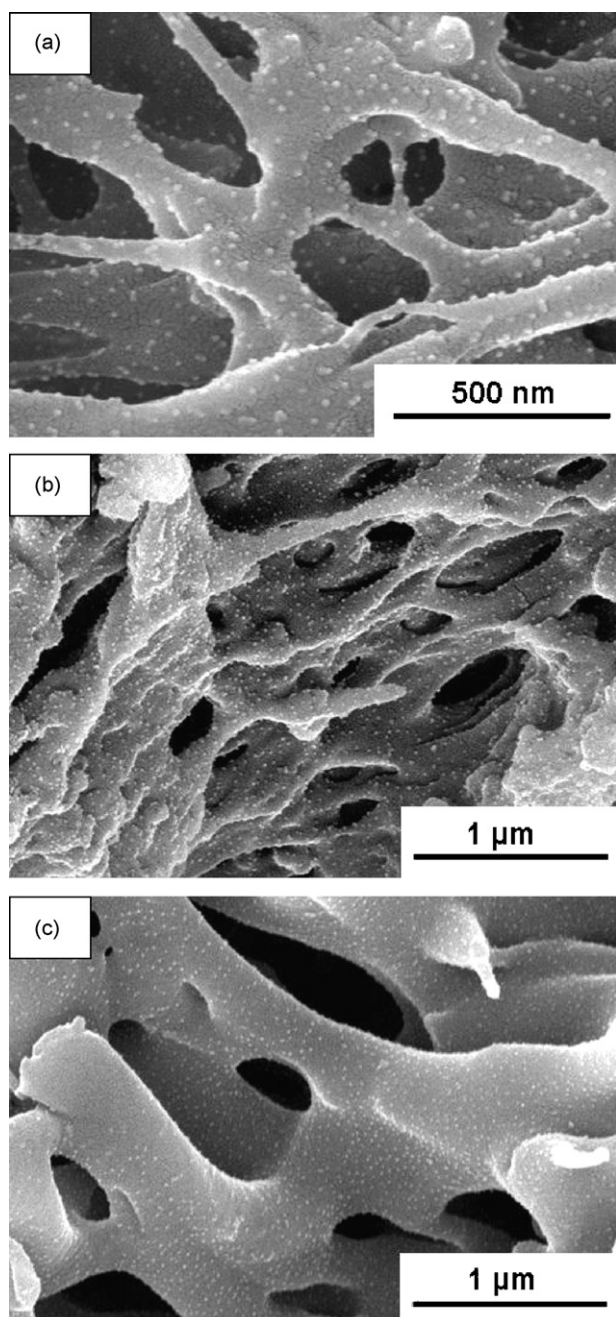
Fig. 4. SEM images of PES hollow fiber membranes coated with PSS/PAH/AuNP films. (a) Shell surface, (b) lumen surface and (c) the interior of the membrane.

3.3. Catalyst loading

SEM provides information on nanoparticle deposition in small spots with image areas of about $10\,\mu m^2$, but such images may not provide a good indication of Au loading on a macroscopic scale. To determine the overall Au content and whether the nanoparticles are evenly distributed along the length of the fiber, coated PES fibers were cut into several pieces, and the nanoparticles in each piece were dissolved in aqua regia for subsequent Au analysis by AAS. Table 1 summarizes these analyses and shows that the Au deposition in the PES fiber is very uniform. Remarkably, the amount of Au in each piece of the fiber differs by less than 8% from the average loading. The average amount of Au in a 5 cm-long PES fiber is 350 nmol, which corresponds to 0.3 mg of Au in a fiber with a length of 22 cm. Gold loading in a PS fiber is $1.2\,\mu mol$ in a 5 cm segment
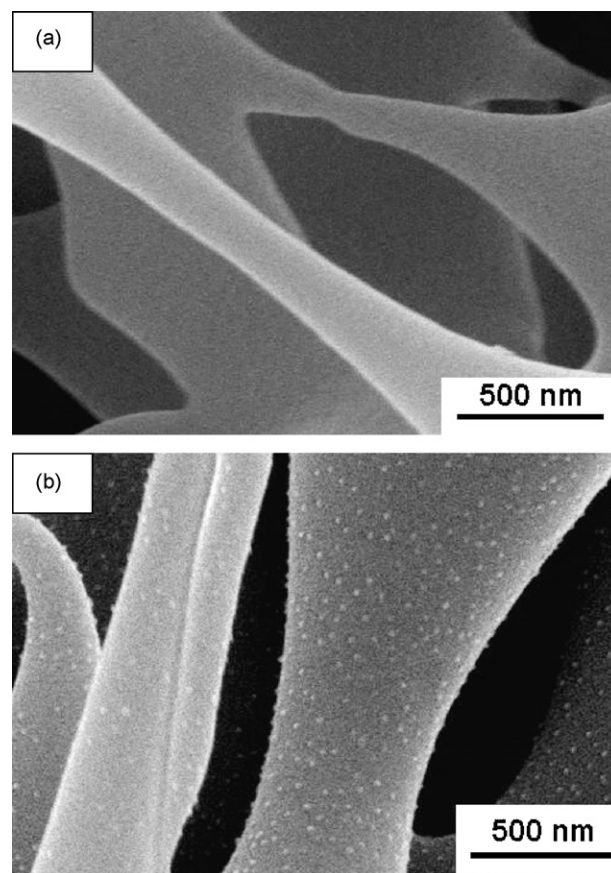

Fig. 5. SEM images of the interior surfaces of (a) a bare PS hollow fiber membrane and (b) a similar membrane coated with a PSS/PAH/AuNP film.

or about 1 mg in a fiber with a length of 22 cm. The higher loading in the PS membranes likely occurs because the cross-sectional area of the walls of these fibers is 5.5 times that in PES fibers. The loading in both types of membranes is comparable to the loading in a chitosan catalytic fiber that was modified by the *in situ* reduction method. In that case, palladium chloride was absorbed on the chitosan and subsequently reduced by hydrogen gas to give a Pd loading of 0.25–2.5 mg in a 50 cm fiber [13].
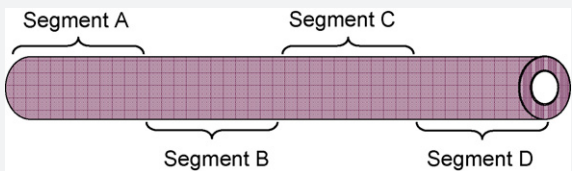
Adsorption of additional PAH/Au nanoparticle bilayers should further increase the Au loading in the film [42]. However, due to challenges with blocking of some membranes by the polyelectrolyte films (see below), the catalytic studies described here focus on modification with only one PAH/AuNP layer.

3.4. Water permeability

Although a previous study showed no detectable plugging of membrane pores during deposition of poly(acrylic acid)/PAH/AuNP films in porous alumina (pore size of $0.2\,\mu m$) [42], the hollow fiber flow configuration and the spongy membrane structure in the present case may lead to pore blockage. Fig. 6 shows the water permeabilities of PES fibers after each step in the deposition of PSS/PAH/AuNP films. (Permeabilities are determined by measuring the pressure dependence of pure water flux in the shell to lumen flow mode). The bare PES fiber exhibits a water permeability of 41 $m^3/(m^2$ day bar), which is in the high range of fluxes through MF membranes [11]. After PSS deposition, water permeability decreases by less than 10%, but adsorption of one bilayer of PSS/PAH reduces permeability by 30% compared to a bare fiber. Moreover, adsorption of Au nanoparticles on the PSS/PAH film results in a water permeability of only 22 $m^3/(m^2$ day bar), about

Table 1
Au loading along PES fibers coated with PSS/PAH/AuNP. The length of each segment is approximately 5 cm.

	Segment A (nmol)	Segment B (nmol)	Segment C (nmol)	Segment D (nmol)	Average (nmol)
Fiber 1[a]	357	371	347	375	363 ± 13
Fiber 2[a]	345	339	326	370	345 ± 18

[a] The reported values are normalized to a fiber length of 5 cm.

half of the value for the bare fiber. This decrease in water permeability is somewhat surprising because typical PSS/PAH films are only 1 nm thick [54,55], and the pores sizes in these membranes are in the range of several hundred nanometers. Comparison of Figs. 4(b) and 3(c) suggests that film deposition partially occludes the lumen surface, which may account for the 50% drop in permeability after deposition of the PSS/PAH/AuNP film.
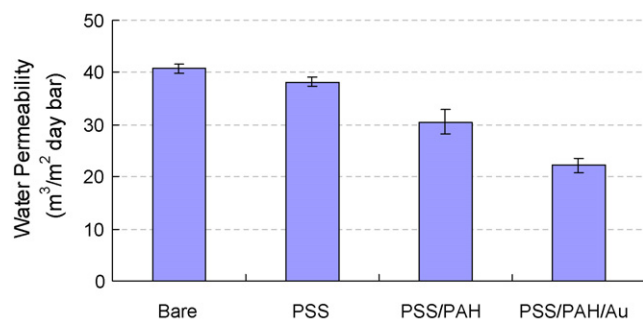
We should note that in some cases adsorption of PSS/PAH/AuNP films in PES fibers decreases flow to around 7% of that before modification. SEM images of different bare fibers indicate that the pore size varies greatly from roll to roll or perhaps with time (see Supplementary data, Fig. S3). As expected, smaller pores are more prone to plugging during film adsorption. To overcome this problem, we employ PS fibers, which have a permeability of 360 m^3/(m^2 day bar). Adsorption of PSS/PAH/AuNP films in these fibers decreases permeability by less than 10%.

3.5. Examination of the catalytic activity of nanoparticle-coated fibers

The reduction of 4-nitrophenol with NaBH$_4$ (Fig. 1) serves as a test reaction for examining the catalytic activity of hollow fibers loaded with Au nanoparticles. This reaction is attractive because it does not proceed in the absence of catalyst, and yet it rapidly occurs in the presence of Au nanoparticles and can be easily monitored by UV–vis spectrophotometry [53,56,57]. Some previous studies examined nitrophenol degradation with chitosan hollow fibers [13,15,58]. In a typical reaction, the feed solution contains 0.5 mM 4-nitrophenol and 25 mM NaBH$_4$ so the amount of the reducing agent is in large excess throughout the reaction.
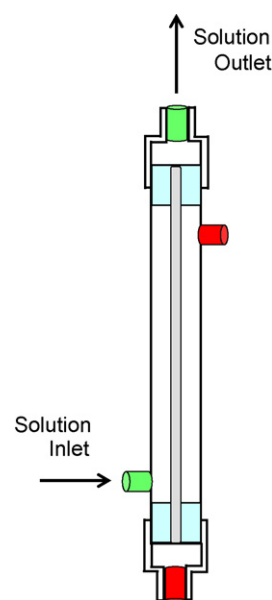
3.5.1. Catalytic reduction using PES fibers modified with PSS/PAH/AuNP films

We first reduced 4-nitrophenol in the lumen–shell flow configuration with the lumen outlet plugged. These reactions initially result in more than 99% reduction of 4-nitrophenol during flow

through PES membranes modified with PSS/PAH/AuNP films [47]. Control experiments with fibers coated with PSS/PAH show less than 1% reduction of 4-nitrophenol under similar conditions. However, in this flow mode the accumulation of H$_2$ in the fiber can potentially cause variations in flux and effective membrane area. (Periodic opening of the fiber outlet causes increases in the transmembrane flux). Thus, all further reactions employ the shell to lumen configuration without cross-flow (Fig. 7). The fiber is perpendicular to the ground, and any trapped hydrogen should pass through the lumen outlet along with the permeate. The red plug on the shell (Fig. 7) can be removed periodically to release H$_2$ that accumulates in the shell. With this flow mode, the permeate flux is 0.7 ± 0.1 mL/(cm^2 min) at an applied pressure of 1.4 bar, and the residence time in the membrane is 210 ± 30 ms.

Fig. 8 shows the extent of 4-nitrophenol reduction during flow (shell to lumen) through a hollow fiber membrane modified with a PSS/PAH/AuNP film. The 4-nitrophenol reduction is more than 99% for 30 min and then decreases to 83% after 1 h. One possible reason for the decline in conversion is that the amount of reducing agent in the feed tank decreases with time due to continuous NaBH$_4$ degradation. A previous study reports that NaBH$_4$ decomposes completely to NaBO$_2$ and hydrogen gas in 20 min at 75 °C [59]. Although the membrane reactions occur at room temperature, an equation developed by Kreevoy suggests that 50% of the NaBH$_4$ should decompose at this temperature in approximately 1 h [60].

Fig. 6. Water permeability of PES hollow fiber membranes before (bare) and after adsorption of different polyelectrolyte films.

Fig. 7. Schematic diagram of the shell to lumen solution flow configuration used in most catalytic reactions in this study. (The two red cylinders represent plugged outlets.)
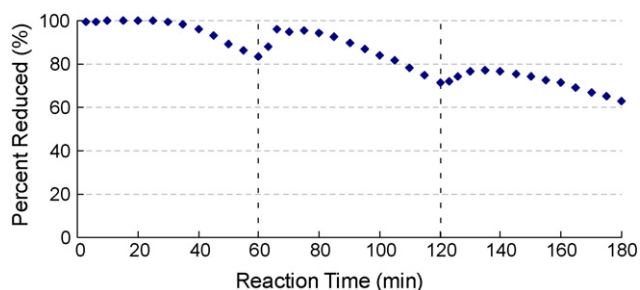
Fig. 8. Percent reduction of 4-nitrophenol during passage of a 0.5 mM 4-nitrophenol, 25 mM NaBH$_4$ aqueous solution through a PES hollow fiber membrane coated with a PSS/PAH/AuNP film. Flow through the membrane occurs in the shell–lumen configuration without cross-flow. The effective fiber length is 22 cm, the fiber shell surface area is 3.45 cm^2, the Au loading is 0.3 mg, the volume passed through the module is about 500 mL, the residence time in the membrane is 210 ± 30 ms and the permeate flux is 0.7 ± 0.1 mL/(cm^2 min). The dashed, vertical lines represent the addition of a fresh 4-nitrophenol/NaBH4 solution.

To minimize the effect of NaBH$_4$ degradation on conversion, the feed solution is replaced every 60 min. Upon replacing the feed solution after 1 h of reaction, 4-nitrophenol conversion recovers from 83% to values as high as 96%, but then begins decreasing again, so conversion is only 70% after 2 h (Fig. 8). When the feed is replaced a second time (after 2 h), the conversion only recovers to 77% and finally drops to 60% after 3 h. The incomplete recovery of conversion after replacing the feed shows that degradation of NaBH$_4$ is not the sole cause for the conversion decline.

A second possible reason for the conversion decline is that reaction by-products [58] block the catalytic sites of the nanoparticles. Comparison of SEM images of the lumen surfaces of modified PES fibers before (Fig. 4(b)) and after the NaBH$_4$/4-nitrophenol reaction (Fig. 9) indicates that deposits form during the reaction. Interestingly, no deposits appear in the fiber wall where most of the catalyst is located. Another possible cause of the conversion decline, catalyst leaching, is discussed in more detail below.

3.5.2. Catalytic reduction using PS fibers modified with PSS/PAH/AuNP films

Reduction of 4-nitrophenol also occurs rapidly when using PSS/PAH/AuNP-modified PS hollow fiber membranes. Fig. 10 shows 4-nitrophenol conversion over a 4 h period in which the feed is replaced after 80 and 180 min. Because of the high permeability of these membranes, the permeate flux is 1.4 ± 0.2 mL/(cm^2 min) under a pressure <0.2 bar. (This flux corresponds to a membrane
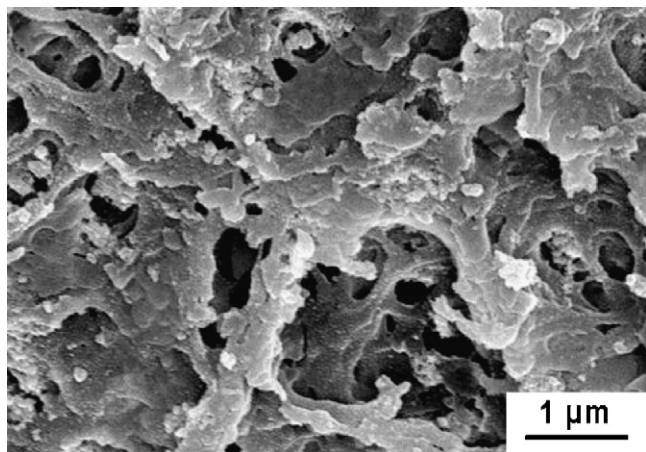

Fig. 9. SEM image of the lumen surface of a catalytic hollow fiber that was employed for reduction of 4-nitrophenol for 3 h. This is the same membrane that was used to obtain the data in Fig. 8.
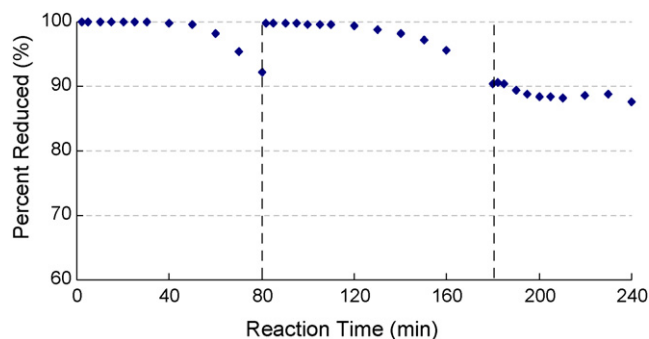

Fig. 10. Percent reduction of 4-nitrophenol during passage of a 0.5 mM 4-nitrophenol, 25 mM NaBH$_4$ aqueous solution through a PS hollow fiber membrane coated with a PSS/PAH/AuNP film. The reaction takes place in the shell–lumen flow configuration without cross-flow using an effective fiber length of 15.5 cm. The fiber shell surface area is 5.84 cm^2, the Au loading is 0.7 mg, the volume passed through the module is about 2000 mL, and the flux through the membrane is 1.4 ± 0.2 mL/(cm^2 min), which corresponds to a membrane residence time of 240 ± 30 ms. The dashed, vertical lines represent the addition of a fresh 4-nitrophenol/NaBH$_4$ solution.

residence time of 240 ± 30 ms.) Conversion is more than 99.9% for the first 30 min and decreases to 92% after 80 min. Once the feed solution is replaced, however, conversion recovers to around 99.9% and remains more than 99% for another 40 min. Conversion drops to 90% after 180 min, and replacing the feed solution a second time does not result in recovery of the catalytic activity.

To determine whether the conversion decline stems from catalyst leaching, the Au concentration in the permeate samples was analyzed by ICP-OES. The permeate contains less than 5 ppb Au throughout the reaction period, which corresponds to <3% cumulative leaching of the Au in the membrane. Hence, Au leaching is not a likely cause for conversion decline in this experiment.

To minimize the effect of NaBH$_4$ degradation on conversion decline, another 4 h 4-nitrophenol reduction was performed where the feed solution (500 mL of 0.5 mM 4-nitrophenol and 25 mM NaBH$_4$) was replaced every 30 min. Fig. 11 shows the plot of conversion vs. reaction time at a flux of 1.4 mL/(cm^2 min). 4-Nitrophenol conversion is at least 99.9% for 90 min and >99.7% for another 65 min. Even after 3 h, more than 99% of the 4-nitrophenol is reduced. However, during the 4 h of reaction, conversion drops to between 95 and 98%. The Au concentration in the permeate samples is again <5 ppb, showing that conversion declines are not due to leaching of Au. The maximum 5% conversion decline is significantly
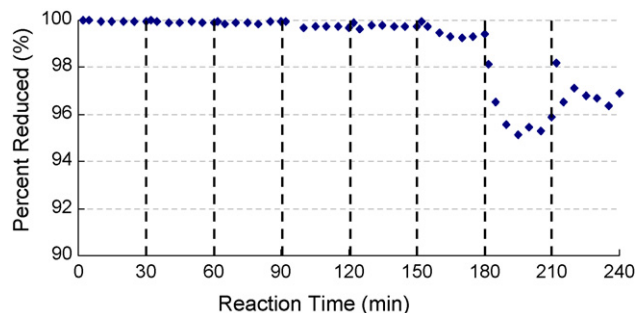

Fig. 11. Percent reduction of 4-nitrophenol during passage of a 0.5 mM 4-nitrophenol, 25 mM NaBH$_4$ aqueous solution through a PS hollow fiber membrane coated with a PSS/PAH/AuNP film. The reaction takes place in the shell–lumen flow configuration without cross-flow using an effective fiber length of 15.5 cm. The fiber shell surface area is 5.84 cm^2, the Au loading is 0.7 mg, the volume passed through the module is about 2000 mL, and the flux through the membrane is 1.4 ± 0.2 mL/(cm^2 min), which corresponds to a membrane residence time of 240 ± 30 ms. The dashed, vertical lines represent the addition of a fresh 4-nitrophenol/NaBH$_4$ solution.

less than the conversion drop of 12% in the experiment where the feed solution is only replaced every 80–100 min (Fig. 10). Conversion declines are less severe when the feed is replaced more often, and when the feed is not replaced, the NaBH$_4$ solution becomes less reducing. Thus, the fouling mechanism may include oxidation of aminophenol [58] in the less reducing solution and formation of polymer products that foul the catalyst.

4. Conclusions

Layer-by-layer adsorption of polyelectrolytes and Au nanoparticles provides a simple and effective way to modify the pores of hollow fibers and prepare catalytic membrane reactors. This procedure results in a dense layer of unaggregated nanoparticles in the membrane pores. Catalytic reduction of 4-nitrophenol with NaBH$_4$ shows that the immobilized nanoparticles are highly active, but their activity declines over time, presumably because of catalyst fouling. The shell–lumen flow configuration is probably better suited for this type of reaction than lumen–shell flow because in the former case gas is less likely to build up in the fiber. Current work focuses on improving catalyst stability, understanding the reaction kinetics, and exploring other catalytic reactions.

Appendix A. Supplementary data

Supplementary data associated with this article can be found, in the online version, at doi:10.1016/j.cattod.2010.02.040.

References

[1] J.S. Butler, B. Gordon, I.R. Harrison, J. Appl. Polym. Sci. 35 (1988) 1183.
[2] H.R. Gao, Y. Xu, S.J. Liao, R. Liu, J. Liu, D.C. Li, D.R. Yu, Y.K. Zhao, Y.H. Fan, J. Membr. Sci. 106 (1995) 213.
[3] H.R. Gao, S.J. Liao, Y. Xu, R. Liu, J. Liu, D.C. Li, Catal. Lett. 27 (1994) 297.
[4] C.Q. Liu, Y. Xu, S.J. Liao, D.R. Yu, Y.K. Zhao, Y.H. Fan, J. Membr. Sci. 137 (1997) 139.
[5] A. Kleinert, A. Feldhoff, T. Schiestel, J. Caro, Catal. Today 118 (2006) 44.
[6] T.A. Peters, J. Fontalvo, M.A.G. Vorstman, J.T.F. Keurentjes, Chem. Eng. Res. Des. 82 (2004) 220.
[7] H. Wang, C. Tablet, T. Schiestel, S. Werth, J. Caro, Catal. Commun. 7 (2006) 907.
[8] R. van der Vaart, V.I. Lebedeva, I.V. Petrova, L.M. Plyasova, N.A. Rudina, D.I. Kochubey, G.F. Tereshchenko, V.V. Volkov, J. van Erkel, J. Membr. Sci. 299 (2007) 38.
[9] H. Jiang, H. Wang, S. Werth, T. Schiestel, J. Caro, Angew. Chem. Int. Ed. Engl. 37 (2008) 9341.
[10] V.I. Lebedeva, V.M. Gryaznov, I.V. Petrova, V.V. Volkov, G.F. Tereshchenko, E.I. Shkol'nikov, L.M. Plyasova, D.I. Kochubey, R. van der Vaart, E.L.J. van Soest-Verecammen, Kinet. Catal. 47 (2006) 867.
[11] M. Mulder, Basic Principles of Membrane Technology, Kluwer Academic Publishers, Dordrecht, 1996.
[12] S.H. Israni, B.K.R. Nair, M.P. Harold, Catal. Today 139 (2009) 299.
[13] F. Peirano, T. Vincent, F. Quignard, M. Robitzer, E. Guibal, J. Membr. Sci. 329 (2009) 30.
[14] J. Caro, K.J. Caspary, C. Hamel, B. Hoting, P. Kolsch, B. Langanke, K. Nassauer, T. Schiestel, A. Schmidt, R. Schomacker, A. Seidel-Morgenstern, E. Tsotsas, I. Voigt, H. Wang, R. Warsitz, S. Werth, A. Wolf, Ind. Eng. Chem. Res. 46 (2007) 2286.
[15] F.P. Blondet, T. Vincent, E. Guibal, Int. J. Biol. Macromol. 43 (2008) 69.
[16] D. Astruc, F. Lu, J.R. Aranzaes, Angew. Chem. Int. Ed. Engl. 44 (2005) 7852.
[17] R. Pool, Science 248 (1990) 1186.
[18] L.D. Pachón, G. Rothenberg, Appl. Organomet. Chem. 22 (2008) 288.
[19] Y. Mei, G. Sharma, Y. Lu, M. Ballauff, M. Drechsler, T. Irrgang, R. Kempe, Langmuir 21 (2005) 12229.
[20] M. Comotti, W.-C. Li, B. Spliethoff, F. Schüth, J. Am. Chem. Soc. 128 (2006) 917.
[21] K.H. Park, K. Jang, H.J. Kim, S.U. Son, Angew. Chem. Int. Ed. Engl. 46 (2007) 1152.
[22] M. Valden, X. Lai, D.W. Goodman, Science 281 (1998) 1647.
[23] Y. Jiang, Q. Gao, J. Am. Chem. Soc. 128 (2006) 716.
[24] D.E. Meyer, D. Bhattacharyya, J. Phys. Chem. B 111 (2007) 7142.
[25] L. Brandao, D. Fritsch, A.M. Mendes, L.M. Madeira, Ind. Eng. Chem. Res. 46 (2007) 5278.
[26] L.-S. Zhong, J.-S. Hu, Z.-M. Cui, L.-J. Wan, W.-G. Song, Chem. Mater. 19 (2007) 4557.
[27] B.C. Gates, Chem. Rev. 95 (1995) 511.
[28] J. Sarkar, V.T. John, J. He, C. Brooks, D. Gandhi, A. Nunes, G. Ramanath, A. Bose, Chem. Mater. 20 (2008) 5301.
[29] E. Nikolla, J. Schwank, S. Linic, J. Am. Chem. Soc. 131 (2009) 2747.
[30] A.J. Akande, R.O. Idem, A.K. Dalai, Appl. Catal. A 287 (2005) 159.
[31] A.I. Kozlov, A.P. Kozlova, K. Asakura, Y. Matsui, T. Kogure, T. Shido, Y. Iwasawa, J. Catal. 196 (2000) 56.
[32] P. Claus, A. Brückner, C. Mohr, H. Hofmeister, J. Am. Chem. Soc. 122 (2000) 11430.
[33] A. Wolf, F. Schüth, Appl. Catal. A 226 (2002) 1.
[34] N. Zheng, G.D. Stucky, J. Am. Chem. Soc. 128 (2006) 14278.
[35] J. Cho, F. Caruso, Chem. Mater. 17 (2005) 4547.
[36] J.W. Ostrander, A.A. Mamedov, N.A. Kotov, J. Am. Chem. Soc. 123 (2001) 1101.
[37] F. Caruso, R.A. Caruso, H. Möhwald, Science 282 (1998) 1111.
[38] C. Jiang, S. Markutsya, V.V. Tsukruk, Langmuir 20 (2004) 882.
[39] S. Kidambi, J. Dai, J. Li, M.L. Bruening, J. Am. Chem. Soc. 126 (2004) 2658.
[40] S. Joly, R. Kane, L. Radzilowski, T. Wang, A. Wu, R.E. Cohen, E.L. Thomas, M.F. Rubner, Langmuir 16 (1999) 1354.
[41] D.M. Dotzauer, S. Bhattacharjee, Y. Wen, M.L. Bruening, Langmuir 25 (2009) 1865.
[42] D.M. Dotzauer, J. Dai, L. Sun, M.L. Bruening, Nano Lett. 6 (2006) 2268.
[43] S. Bhattacharjee, M.L. Bruening, Langmuir 24 (2008) 2916.
[44] S. Bhattacharjee, D.M. Dotzauer, M.L. Bruening, J. Am. Chem. Soc. 131 (2009) 3601.
[45] S. Kidambi, M.L. Bruening, Chem. Mater. 17 (2004) 301.
[46] M. Schönhoff, J. Phys.: Condens. Matter 15 (2003).
[47] J. Macanás, L. Ouyang, M.L. Bruening, M. Muñoz, J.C. Remigy, J.F. Lahitte, Catal. Today 156 (2010) 100.
[48] B.V. Enüstün, J. Turkevich, J. Am. Chem. Soc. 85 (1963) 3317.
[49] S. Kumar, K.S. Gandhi, R. Kumar, Ind. Eng. Chem. Res. 46 (2007) 3128.
[50] S. Rouaix, C. Causserand, P. Aimar, J. Membr. Sci. 277 (2006) 137.
[51] R. Malaisamy, M.L. Bruening, Langmuir 21 (2005) 10587.
[52] N.A. Kotov, Nanostruct. Mater. 12 (1999) 789.
[53] N. Pradhan, A. Pal, T. Pal, Colloids Surf. A 196 (2002) 247.
[54] L. Ouyang, R. Malaisamy, M.L. Bruening, J. Membr. Sci. 310 (2008) 76.
[55] M.D. Miller, M.L. Bruening, Chem. Mater. 17 (2005) 5375.
[56] K. Esumi, K. Miyamoto, T. Yoshimura, J. Colloid Interface Sci. 254 (2002) 402.
[57] S.K. Ghosh, M. Mandal, S. Kundu, S. Nath, T. Pal, Appl. Catal. A 268 (2004) 61.
[58] T. Vincent, E. Guibal, Langmuir 19 (2003) 8475.
[59] L. Soler, J. Macanás, M. Muñoz, J. Casado, Int. J. Hydrogen Energy 32 (2007) 4702.
[60] M.M. Kreevoy, R.W. Jacobson, Ventron Alembic 15 (1979) 2.